Available online at www.sciencedirect.com
ScienceDirect
Journal of Power Sources 176 (2008) 82–89
JOURNAL OF POWER SOURCES
www.elsevier.com/locate/jpowsour

Electrical conductivity and performance of doped $LaCrO_3$ perovskite oxides for solid oxide fuel cells

San Ping Jiang [a,*], Li Liu [a], Khuong P. Ong [b], Ping Wu [b], Jian Li [c], Jian Pu [c]

[a] *School of Mechanical and Aerospace Engineering, Nanyang Technological University, Singapore 639798, Singapore*
[b] *Institute of High Performance Computing, 1 Science Park Road, Singapore 117528, Singapore*
[c] *School of Materials Science and Engineering, Huazhong University of Science and Technology, Wuhan 430074, China*

Received 27 July 2007; accepted 11 October 2007
Available online 25 October 2007

Abstract

The crystalline structure, redox stability and electrical conductivity of $LaCrO_3$, $(La_{1-x}M_x)CrO_3$ (M = Mg, Ca, Ba for $x = 0.3$ and M = Sr for $x = 0.25$), and $(La_{0.75}Sr_{0.25})(Cr_{0.5}Mn_{0.5})O_3$ (LSCM) perovskites are studied from 500 to 800 °C in both oxidizing and reducing atmospheres. Dopability, redox stability and electrical conductivity are compared and examined. A-site doping with alkaline elements is found to improve significantly the electrical conductivity, particularly if properly doped. The highest conductivity is obtained with Ca- and Sr-doped $LaCrO_3$. A-site doping also reduces the activation energy of the electrical conductivity, particularly under a reducing environment. Preliminary electrochemical results indicate that Ca-doped $LaCrO_3$ shows promise as a cathode for solid oxide fuel cells.

Keywords: Solid oxide fuel cell; Doped lanthanum chromites; Conductivity; Redox stability; Electrochemical performance

1. Introduction

Solid oxide fuel cells (SOFCs) are a subject of vigorous research as a new power generation technology due to their low-greenhouse gas emissions, high efficiency and fuel flexibility. A SOFC stack has four basic components: Ni-yttria stabilized zirconia (Ni-YSZ) cermet anode, YSZ electrolyte, $(La,Sr)MnO_3$ cathode, and $LaCrO_3$ interconnect [1]. A Ni-YSZ cermet anode works well when fed by hydrogen, but suffers from coking and sulfur poisoning when fed by natural gas, which is a more readily accessible fuel [2]. Hence, considerable efforts are being made world-wide to develop a SOFC that operates directly with hydrocarbon fuels such as natural gas.

Two approaches are generally being explored: (i) internal-reforming of natural gas to form syngas (H_2 and CO) or (ii) using alternative anode materials with high-electrocatalytic activity to oxidize directly methane and high resistance and tolerance towards carbon deposition and sulfur poisoning. In the second approach, lanthanum chromite-based perovskites attract special interest and yield some promising results [3–8]. Tao and Irvine [3] investigated the electrochemical activities of the quadruple oxide, $(La,Sr)(Cr,Mn)O_3$ (LSCM), as a SOFC anode material and found that the power performance of a single cell fed by methane was comparable to a standard cell with a Ni-YSZ cermet anode when fed by H_2. Our recent studies [6,7] have shown that LSCM/YSZ composite anodes have low activity towards carbon deposition and the electrocatalytic activity can be significantly enhanced by impregnation of nano-sized Gd-doped ceria particles. LSCM/YSZ composites also show reasonable electrocatalytic activity for the oxygen reduction reaction [9].

In this work, we examine in detail the effect of A-site doping on the electrical properties of lanthanum chromite oxides with special reference to potential application as SOFC electrodes. Besides Sr, alkaline earth (AE) elements such as Mg, Ca and Ba are chosen as A-site dopants in $LaCrO_3$. For the purpose of comparison, the electrical conductivity of $(La,Sr)(Cr,Mn)O_3$ is also studied. The effect of doping and microstructure on the electrical conductivity properties of the lanthanum chromites is discussed.

* Corresponding author. Tel.: +65 6790 5010; fax: +65 6792 4062.
E-mail address: mspjiang@ntu.edu.sg (S.P. Jiang).

0378-7753/$ – see front matter © 2007 Elsevier B.V. All rights reserved.
doi:10.1016/j.jpowsour.2007.10.053

2. Experimental

$LaCrO_3$ and $(La_{1-x}M_x)CrO_3$ (M = Mg, Ca, Ba for $x = 0.3$ and M = Sr for $x = 0.25$) powders were prepared by the conventional solid-state reaction method. The starting chemical powders were La_2O_3 (Sigma–Aldrich, 99.9%), MgO (Fluka, >98%), $CaCO_3$ (Fluka, >99%), $SrCO_3$ (Merck, precipitated), $BaCO_3$ (Fluka, >98.5%), Cr_2O_3 (Merck, anhydrous) and $MnCO_3$ (Sigma–Aldrich, 99.9%). Given amounts of the starting raw chemicals were weighed and ball milled for 4 h and then calcined at 1200 °C. The resulting powders were pressed uniaxially into a bar of dimensions 26 mm × 8 mm × 5 mm and sintered at 1600 °C for 5 h in air $(La_{0.75}Sr_{0.25})(Cr_{0.5}Mn_{0.5})O_3$ (LSCM) powder was prepared and sintered under the same temperature.

Conductivity (σ) measurements were performed with a four-probe d.c. method within a temperature range from 500 to 800 °C in oxidizing (air) and a reducing (10 vol.% H_2/90% N_2) environment. Platinum paste was used as a current-collector and Pt wire was used as current and voltage probes. The voltage was measured under a constant current. The measurement in air was started from 500 °C and increased to 800 °C with a step size of 50 °C. The atmosphere was then switched to 10% H_2/N_2 and the electrical conductivity was measured from 800 to 500 °C with a step size of 100 °C. At each step, the temperature was held until the measured voltage became stable.

Preliminary electrochemical measurements were taken on selected doped $LaCrO_3$ in a three-electrode, half-cell polarization test. Doped $LaCrO_3$ electrodes were applied to YSZ discs by slurry painting and sintered at 1200 °C in air for 2 h. Platinum paste was painted on to the other side of the electrolyte disc to make the counter and reference electrodes. Platinum mesh was used as the current-collector for both the working and the counter electrodes. The airflow rate was 100 mL min^{-1}. Electrochemical impedance spectra of the cathodes were recorded at open-circuit with a 10 mV signal amplitude over the frequency range 0.01 Hz to 1 MHz, using a Solartron 1260 frequency response analyzer in conjunction with a 1287 electrochemical interface. The electrode interface (polarization) resistance (R_E) was directly measured from the differences between the low and high frequency intercepts on the impedance axis.

X-ray diffraction (Philips MPD 1880 Diffractometer) was employed to characterize the crystalline structure and existence of the dopant phase in powders after calcination. The phase change before and after the conductivity measurement in a reducing atmosphere was also examined. Scanning electron microscopy (Leica S360) was used to examine the microstructure of the specimens. Thermal expansion coefficients (TEC) of the materials were also examined by thermomechanical analysis (TMA 2940, TA Instruments).

3. Results and discussion

3.1. XRD characterization

Fig. 1 shows XRD spectra for the perovskite oxides before and after conductivity measurement in 10% H_2/N_2 $(La_{0.75}Sr_{0.25})CrO_3$, $(La_{0.70}Ba_{0.30})CrO_3$ and LSCM have a R3-C symmetry, while $LaCrO_3$ and $(La_{0.70}Ca_{0.30})CrO_3$ are in space group Pnma. Among the AE elements under the present study, the ionic radius of Ca is closest to that of La [10]. This may account for the fact that $(La_{0.70}Ca_{0.30})CrO_3$ and $LaCrO_3$ share the same space group. When larger cations are doped into the $LaCrO_3$ lattice, especially at high concentration, significant lattice distortion will result in reorganization of the ions and hence different symmetry of the lattice. The phase at room temperature changes from hexagonal to rhomohedral polymorphs (both with R3-C symmetry) in Sr-doped $LaCrO_3$ when the Sr doping concentration increases beyond 20 at.% [11,12].

Most powders show a perovskite structure within the sensitivity of XRD measurement, except Mg- and Ba-doped $LaCrO_3$. In the case of $(La_{0.70}Mg_{0.30})CrO_3$, $MgCr_2O_4$, spinel phase was detected in addition to the perovskite phase, probably due to the small ionic size of Mg. The ionic radius of Mg with a coordination number (CN) of 8 is 0.89 Å [10], i.e., about 23.3% smaller than the La^{3+} with the same CN ($r^{VIII}_{La^{3+}}$, 1.16 Å). Considering the Goldschmidt tolerance factor $t = r_A + r_O/\sqrt{2}(r_B + r_O)$ for a perovskite structure [13], the ionic radius available for Mg^{2+} can only bring the tolerance factor to slightly higher than 0.8, i.e., significantly below unity. This indicates a rather high mismatch between the bond lengths and a large distortion of the perovskite structure. Thus, the small Mg cation has preference to occupy the B-site rather than the A-site in $LaCrO_3$, as confirmed by the first-principle defect structure calculation [14]. In the literature, Mg^{2+} is often chosen to dope the B-site [15–19]. Hence, doping Mg results in a deficiency of A-site cations. Even though the perovskite structure is known to be able to accommodate cation or anion deficiency to some extent, the extra B-site cations dissolve from the perovskite lattice, to form a $MgCr_2O_4$ secondary phase.

A high mismatch between bond lengths does not apply to Ba-doped $LaCrO_3$. The ionic radius of Ba^{2+} ($r^{XII}_{Ba^{2+}}$ 1.61 Å) [10] yields a tolerance factor of 1.06, which is close to unity. In fact, $BaCrO_3$ does have a perovskite structure. The secondary phase ($BaCrO_4$ also in Pnma) is probably due to the limited solubility of Ba in the $LaCrO_3$ perovskite lattice. To clarify the solubility limit of Ba in the $LaCrO_3$ structure, powders with lower doping levels (5 and 10 mol%) of Ba in $LaCrO_3$ were prepared and calcined at 1200 °C for 5 h in air. Fig. 2 shows the XRD patterns of (La,Ba)CrO_3 with different Ba doping levels. $(La_{0.95}Ba_{0.05})CrO_3$ shows only a perovskite phase and as the Ba concentration increased to 10 mol%, additional XRD peaks are detected (Fig. 2b). The additional XRD peaks are identified as the $BaCr_2O_4$ phase [20]. This indicates that the solubility of Ba in $LaCrO_3$ is probably below 10 mol%.

To study the redox stability of the perovskite powders, bar samples after sintering were ground to powders and exposed to 10% H_2/N_2 at 800 °C for 12 h. The powders were then characterized by means of XRD and the results are presented in Fig. 3. No visible decomposition of the chromite oxides under the conditions of this study was observed, which indicates the high-redox stability of the materials. In particular, in the case of Ba-doped $LaCrO_3$ the peaks associated with the secondary $BaCr_2O_4$ phase become less significant after exposure in a reducing environment

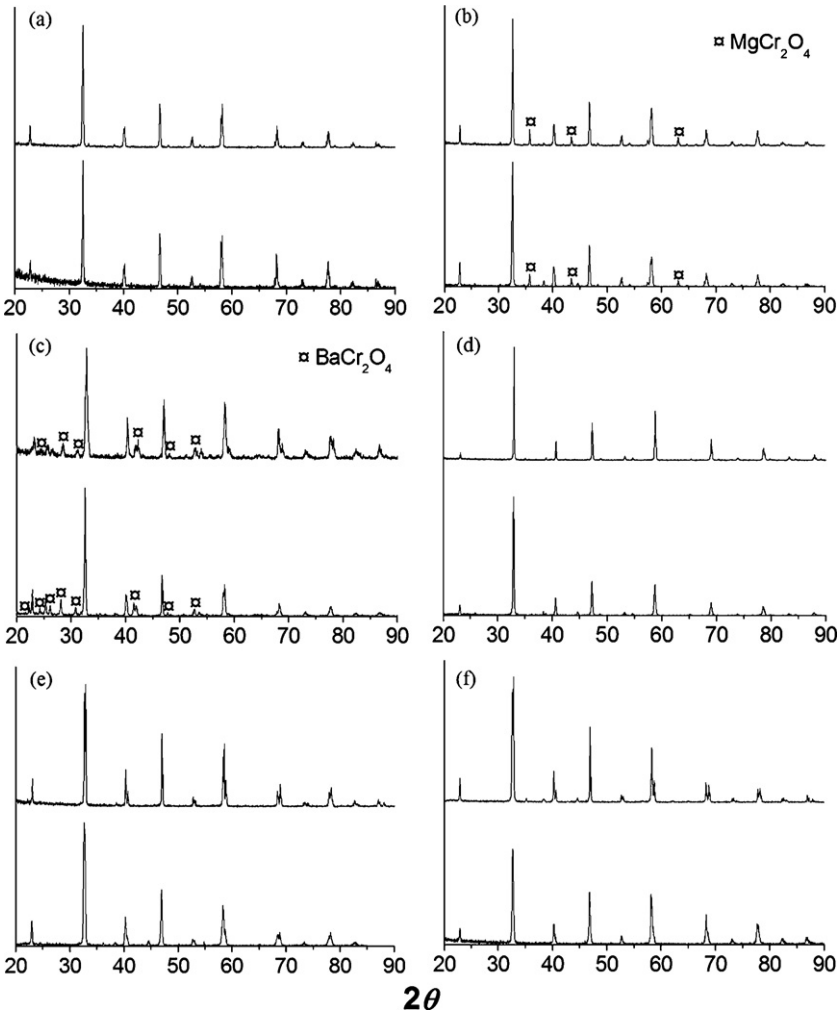

Fig. 1. XRD spectra for perovskite oxides before (upper spectrum) and after (lower spectrum) conductivity measurement in 10% H_2/N_2: (a) $LaCrO_3$, (b) $(La_{0.7}Mg_{0.3})CrO_3$, (c) $(La_{0.7}Ca_{0.3})CrO_3$, (d) $(La_{0.7}Ba_{0.3})CrO_3$, (e) $(La_{0.75}Sr_{0.25})CrO_3$ and (f) $(La_{0.73}Sr_{0.25})(Cr_{0.5}Mn_{0.5})O_3$.

for a short period. This may indicate the increased solubility of Ba in $LaCrO_3$ under a reducing environment.

The redox stability of doped chromites is probably due to the high-chemical stability of Cr^{3+} at the B-site of the perovskite among the first row transition metal system ($Cr^{3+} > Fe^{3+} > Mn^{3+} > Co^{3+}$) [21,22]. Redox stability provides these materials with the potential to be used as anodes for SOFCs.

3.2. Conductivity measurement

The conductivity of doped $LaCrO_3$ was measured in the temperature range of 500–800 °C in air and in 10% H_2/N_2. Fig. 4 shows typical time responses of a doped $LaCrO_3$ (e.g., LSCM) as a function of temperature change in air and in 10% H_2/N_2. The responses were relatively fast, which demonstrates a quick establishment of the equilibrium with the increase in temperature. But there is a significant drop in conductivity when the atmosphere is switched to 10% H_2/N_2 (Fig. 4b). The responses are relatively slower compared with that in air, probably due to the slow kinetics of the surface reaction with H_2.

As shown in Fig. 4, the conductivity of doped $LaCrO_3$ increases with increase in temperature, indicating a thermal-activated process. The activation energy can thus be calculated according to:

$$\sigma T = A \exp\left(-\frac{E_a}{RT}\right) \quad (1)$$

in which E_a is the activation energy, R and T are the gas constants and the absolute temperature, respectively. Fig. 5 is the activation energy plots of the conductivity values of the oxides measured in air and in 10% H_2/N_2. As the Mg cation has preference to occupy the B-site rather than the A-site in $LaCrO_3$ [14], the conductivity for Mg-doped $LaCrO_3$ is not shown in figure. Nevertheless, the conductivity values for a nominal composition of $(La_{0.7}Mg_{0.3})CrO_3$ are low. For example, at 800 °C, the measured conductivity of $(La_{0.7}Mg_{0.3})CrO_3$ is 2.21 and 0.11 S cm^{-1} in air and in 10% H_2/N_2, respectively. The activation energy calculated from the slopes of the curve and the conductivity at 800 °C are listed in Table 1, for both oxidizing and reducing environments.

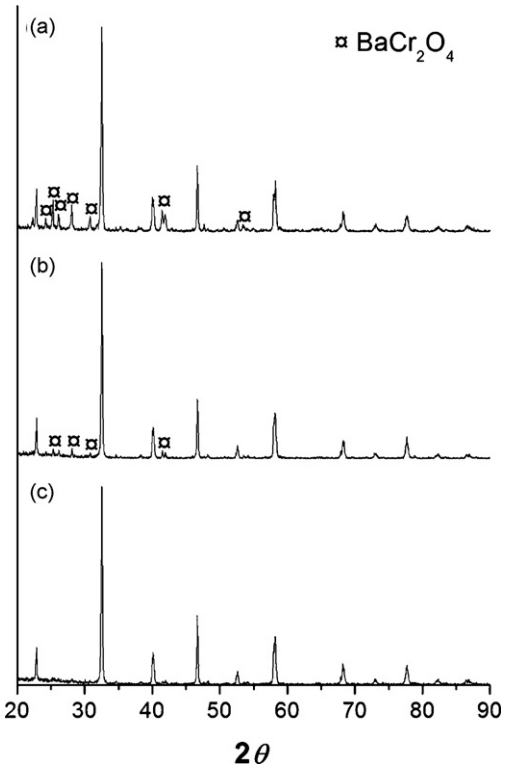

Fig. 2. XRD spectra of $(La_{1-x}Ba_x)CrO_3$ with different Ba doping levels of (a) 5 mol%, (b) 10 mol% and (c) 25 mol%.

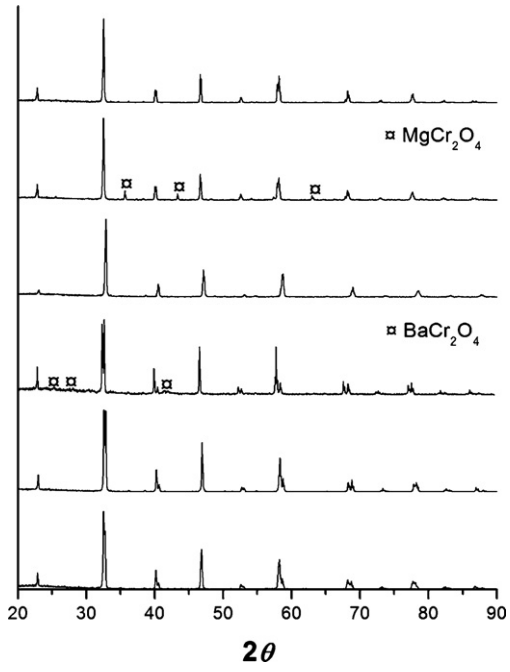

Fig. 3. XRD spectra for perovskite oxide powders after redox stability tests in 10% H_2/N_2 at 800 °C for 12 h: (a) $LaCrO_3$, (b) $(La_{0.7}Mg_{0.3})CrO_3$, (c) $(La_{0.7}Ca_{0.3})CrO_3$, (d) $(La_{0.7}Ba_{0.3})CrO_3$, (e) $(La_{0.75}Sr_{0.25})CrO_3$ and (f) $(La_{0.73}Sr_{0.25})(Cr_{0.5}Mn_{0.5})O_3$.

Pure $LaCrO_3$ is a p-type conductor [23,24]. As Cr^{3+} is able to maintain a six-fold coordination (CN = 6) with oxide ions [3], little anion deficiency, and hence little contribution from ionic charge carriers to the conduction, can be expected. Earlier studies on undoped $LaCrO_3$ indicate that their electrical conductivities are essentially due to the 3d band of the Cr ions through the formation of cation vacancies [25,26]. Even though an oxide-ionic leak current was proposed for the $LaCrO_3$ separator in the O_2 potential gradient [27], only steady-state properties are considered in this work. Hence, in our discussion in A-site doping, we will focus on the electronic conduction within the electronic band structure frame.

From Table 1, the conductivity of pure $LaCrO_3$ perovskite is quite low in either an oxidizing or a reducing environment. In general, doping AE elements at the A-site in $LaCrO_3$ does improve the σ value of the oxide. Especially, doping Ca and Sr at the A-site enhances the σ value by two orders of magnitude. Doping bivalent AE elements may introduce a Cr^{3+} to Cr^{4+} transition [18] and hence more electronic holes in the valence band maximum primarily composed by O-2p level, which is a common process for a charge-transfer type insulator with redox transition metals like Cr and Mn. Recent *ab initio* calculations of the electronic structure of $La_{1-x}M_xCrO_{3-x/2}$ with M = Ca, Sr and Ba show that doping Ca, Sr and Ba will increase the charge population near the top of the valence band and reduce the energy band gap of $LaCrO_3$, resulting in an improvement in the electrical conductivity [28].

With an increase in the charge carriers in the material, the electronic conductivity, the product of carrier mobility (μ) and concentration (n), is expected to increase. However, with a heavy doping of 25%, the effect of doping on the conductivity depends not only on the compensate ion effect due to the interaction between μ and n, but also on the strain caused by the high-doping level. When Ba is doped into the $LaCrO_3$ lattice, large

Table 1
Conductivity and activation energy measured in air and in 10% H_2/N_2 in temperature range of 500–800 °C; $\sigma'_{800\,^\circ C,\,corr}$ is porosity-corrected conductivity values and thermal expansion coefficients (TEC) are measured from 300 to 1000 °C in air

Oxides	$\sigma_{800\,^\circ C}$ (S cm^{-1})		$\sigma'_{800\,^\circ C,corr}$ (S cm^{-1})		E_a (J mol^{-1})		Impurity	Relative density (%)	TEC ($\times 10^{-6}$ °C^{-1})
	Air	10% H_2	Air	10% H_2	Air	10% H_2			
$LaCrO_3$	0.33	0.09	0.96	0.26	19.1	138.0		67	11.3
$(La_{0.7}Mg_{0.3})CrO_3$[a]	2.21	0.11	3.35	0.17	15.9	93.6	$MgCr_2O_4$	83	9.9
$(La_{0.7}Ca_{0.3})CrO_3$	35.1	1.12	50.1	1.6	10.5	38.3		85	11.5
$(La_{0.7}Ba_{0.3})CrO_3$	2.26	–	2.69	–	14.4	–	$BaCr_2O_4$	92	12.5
$(La_{0.75}Sr_{0.25})CrO_3$	26.0	3.11	59.1	7.07	10.0	32.0		72	11.6
$(La_{0.75}Sr_{0.25})(Cr_{0.5}Mn_{0.5})O_3$	25.3	0.20	28.8	0.22	26.1	67.8		>94	12.0

[a] Mg cation has preference to occupy the B-site rather than A-site in $LaCrO_3$ [14].

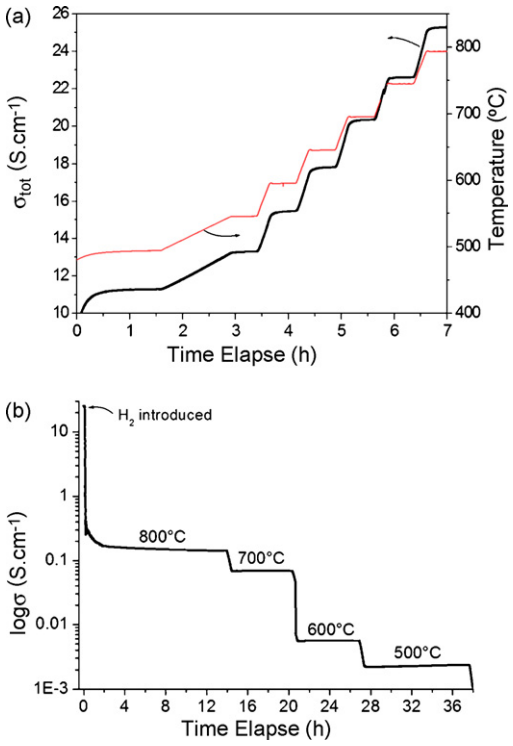

Fig. 4. Typical time responses of $(La_{0.73}Sr_{0.25})(Cr_{0.5}Mn_{0.5})O_3$ as a function of temperature change in (a) air and (b) 10% H_2/N_2.

strain can be expected as the ionic radius of Ba ($r^{XII}_{Ba^{2+}}$, 1.61 Å) is about 18.4% larger than that of La ($r^{XII}_{La^{2+}}$, 1.36 Å). The large mismatch between the La lattice and the doped Ba could introduce distortion of the lattice, which may increase the scattering effect of the charge carriers and hence decrease the conductivity. This is also true for doping with Mg, which has an ionic radius of 0.89 Å, i.e., about 23.3% smaller than that of La^{3+} with the same coordination number ($r^{VIII}_{La^{3+}}$, 1.16 Å). Furthermore, as indicated by XRD analysis, the existence of secondary phases in both $(La_{0.70}Mg_{0.30})CrO_3$ and $(La_{0.70}Ba_{0.30})CrO_3$ may introduce another scattering mechanism for the charge carriers and further reduce the electrical conductivity. Both lattice distortion and the existence of secondary phases explain the relatively low improvement in the electrical conductivities in Mg- and Ba-doped $LaCrO_3$ (Table 1).

Among all the perovskite oxides in this study, Ca- and Sr-doped $LaCrO_3$ have the highest σ values, namely, at least two orders of magnitude higher than that of undoped $LaCrO_3$. The activation energy of the electrical conductivity of undoped and doped $LaCrO_3$ is in the range of 10–20 kJ mol^{-1}, similar to the activation energy reported for other lanthanide chromites [29]. On the other hand, the relatively high activation energy of $(La_{0.75}Sr_{0.25})(Cr_{0.50}Mn_{0.50})O_3$ may indicate a different role played by A- and B-site cations. The different roles played by A- and-B site (transition metals) ions on the physical properties of perovskites has been well explained in a ZSA (Zaanen–Sawatzky–Allen) framework [24,30–33] and further confirmed by electronic band structure and density of states calculations [34–37].

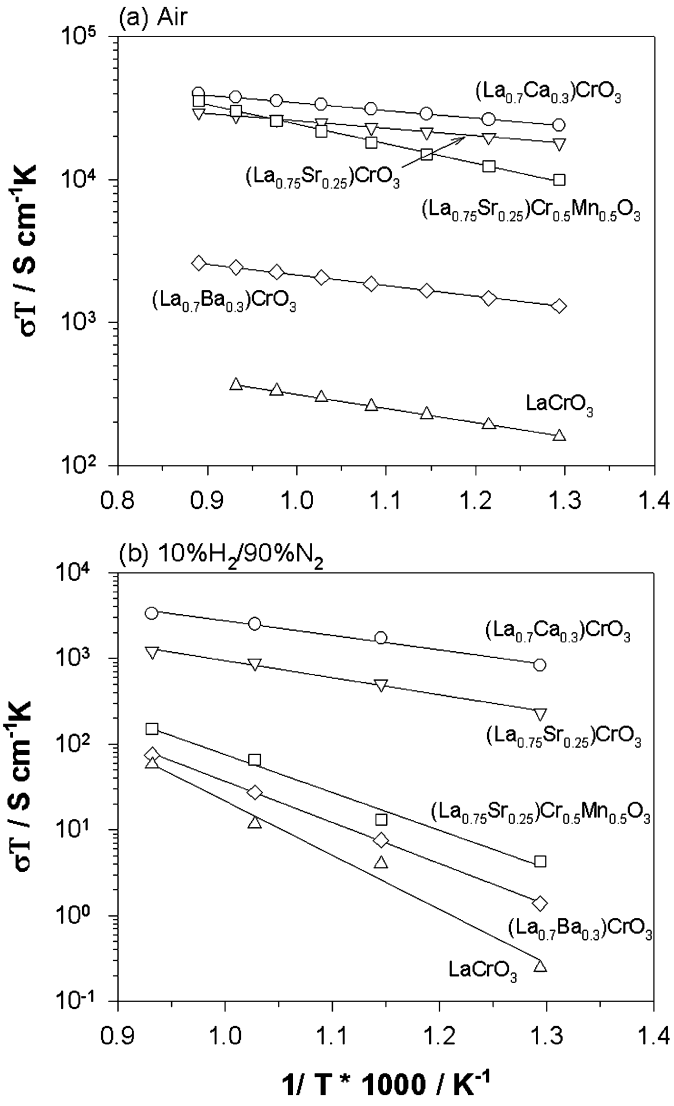

Fig. 5. Activation energy plots of electrical conductivity for undoped $LaCrO_3$, doped $LaCrO_3$, and $(La_{0.73}Sr_{0.25})(Cr_{0.5}Mn_{0.5})O_3$ perovskites in (a) air and (b) 10% H_2/N_2.

In a reducing environment, all oxides show significantly reduced electrical conductivity compared with that in air (Fig. 5b). A decrease in conductivity is commonly observed in p-type conductors when the oxygen partial pressure is reduced, probably due to the easier formation and hence higher concentration of oxygen vacancies under a reducing environment. Acting as a donor, an oxygen vacancy partially decreases the effect of AE doping on the electrical conductivity of $LaCrO_3$. It is noticed that Ca-doped $LaCrO_3$ shows the highest conductivity, consistent with the observation of Mori et al. [18] for A-site doping in lanthanum chromites. As mentioned in [18], the reason may be related to the difference in the formation energy of oxygen vacancies in Sr- and Ca-doped $LaCrO_3$. In the case of LSCM, the electrical conductivity decreases dramatically in 10% H_2/N_2 (two orders of magnitude) in comparison with the A-site doped $LaCrO_3$ (a reduction by one order of magnitude). If the relation between the decrease in conductivity and oxygen vacancy formation is valid, the result shows a higher capability of Cr^{3+} ions

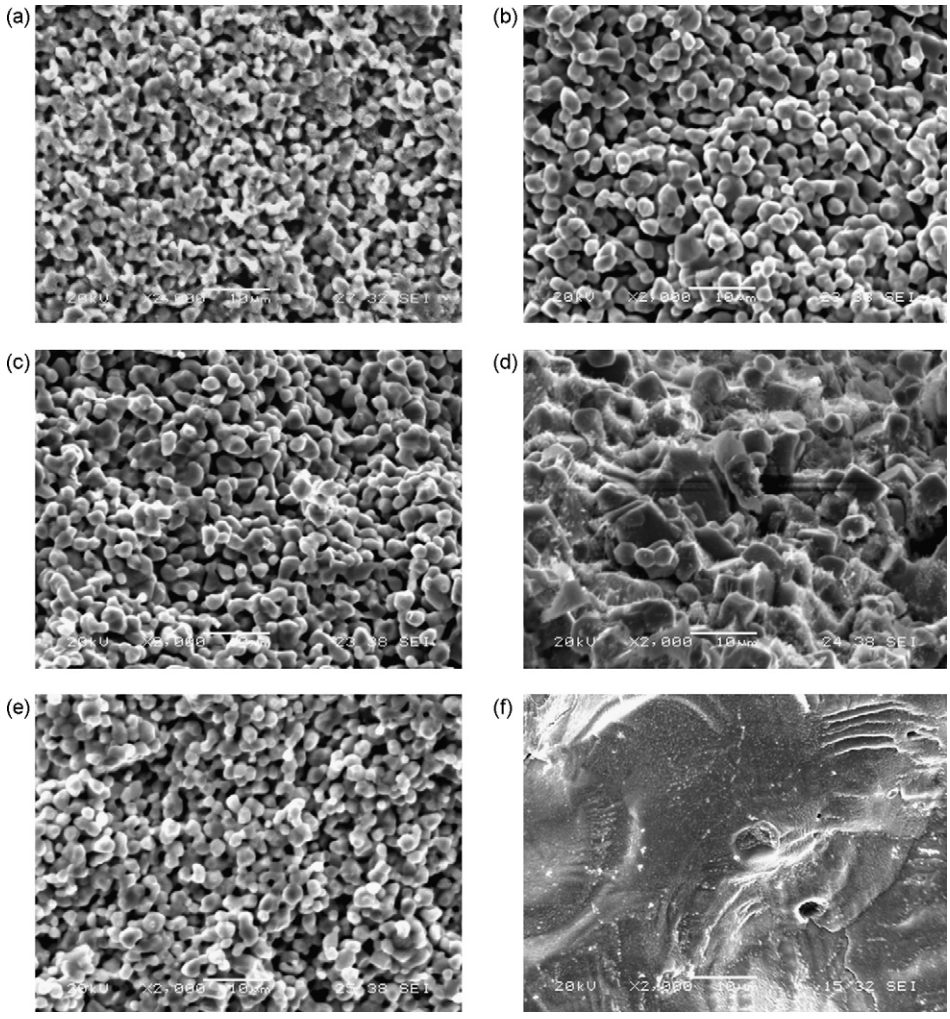

Fig. 6. SEM micrographs of perovskite oxide specimens sintered at 1600 °C for 5 h in air: (a) $LaCrO_3$, (b) $(La_{0.7}Mg_{0.3})CrO_3$, (c) $(La_{0.7}Ca_{0.3})CrO_3$, (d) $(La_{0.7}Ba_{0.3})CrO_3$, (e) $(La_{0.75}Sr_{0.25})CrO_3$ and (f) $(La_{0.73}Sr_{0.25})(Cr_{0.5}Mn_{0.5})O_3$.

to maintain a six-fold coordination with oxide ions than that of Mn^{3+} ions.

3.3. Microstructure and preliminary electrochemical results

Fig. 6 shows SEM micrographs of various oxide conductivity specimens after sintering at 1600 °C for 5 h in air. It is noted that undoped and A-site doped $LaCrO_3$ samples are porous and LSCM is much denser. This shows that lanthanide chromites have poor sinterability and are very difficult to densify under atmospheric conditions. Thesa results also suggest that Mn-doping at the B-site significantly promotes the sintering of lanthanum chromites. The porosity of the samples was estimated by analyzing the cross-section SEM image of each sample with Image-Pro Plus, an image analyzing software. The relative densities were estimated as the average ratio of solid to total area of several SEM images and the results are listed in Table 1. Samples with only chromium at the B-site are rather porous with relative density values lower than 90%. Hence, the true σ of the doped chromites would be higher than the measured values. However, the effect of porosity on the σ values can be taken into account by correcting the measured apparent conductivity (σ_{app}) by means of the following equation [38]:

$$\sigma_{corr} = \frac{\sigma_{app}}{2\,(d_{rel}/100 - 0.5)} \quad (2)$$

where σ_{corr} is the porosity-corrected conductivity and d_{rel} is the relative density. The corrected σ values at 800 °C are also given in Table 1. In general, the magnitude of σ_{corr} and σ values is more or less the same.

As shown in Table 1, doping at the A-site reduces the activation energy of the electrical conductivity in 10% H_2/N_2, while the effect on the activation energy of electrical conductivity in air is relatively small. In the case of A-site doping, E_a is related to the AE acceptor level and to the activation energy for mobility [24]. As undoped and doped $LaCrO_3$ perovskites are p-type conductors with O-2p as the valence band maximum, E_a may mainly reflect the relative positions of defect levels. On the other hand, substituting Mn for 50% Cr at the B-sites in $(La_{0.75}Sr_{0.25})CrO_3$ increases the activation energy of the electrical conductivity in 10% H_2/N_2 in comparison with that of $(La_{0.75}Sr_{0.25})CrO_3$ (E_a is 67.8 kJ mol^{-1} for LSCM and 32 kJ mol^{-1} for Sr-doped

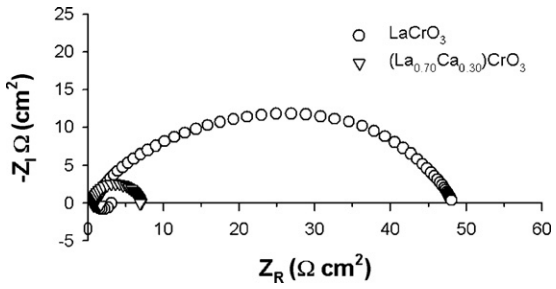

Fig. 7. Electrochemical impedance responses measured on $LaCrO_3$ and $(La_{0.70}Ca_{0.30})CrO_3$ at 800 °C in air. The cathodes sintered at 1200 °C in air for 2 h.

$LaCrO_3$). The variation in E_a for doped lanthanum chromites may also suggest that doping at the A-site plays a different role from that of doping at the B-site. E_a for the doped $LaCrO_3$ perovskites in a reducing environment is much higher than that in air. This could result from the effect of oxygen vacancy formation.

Finally, preliminary measurements were made of the electrochemical performance of $LaCrO_3$ and $(La_{0.70}Ca_{0.30})CrO_3$. Fig. 7 shows the impedance responses for the oxygen reduction reaction on $LaCrO_3$ and $(La_{0.70}Ca_{0.30})CrO_3$ cathodes at 800 °C in air. The impedance responses for this reaction on undoped and Ca-doped $LaCrO_3$ are characterized by a depressed arc, an indication of multi-step processes. For the reaction on undoped $LaCrO_3$, the electrode polarization resistance is 45.3 Ω cm^2 whereas it is 6.3 Ω cm^2 on Ca-doped $LaCrO_3$. The substantially reduced electrode polarization resistance for oxygen reduction on $(La_{0.70}Ca_{0.30})CrO_3$, in comparison with that on $LaCrO_3$, indicates that A-site doping enhances the electrocatalytic activity of the lanthanum chromites for fuel cell reactions. As shown by Ruiz-Morales et al. [9], the electrocatalytic activity of doped lanthanum chromite electrodes can also be significantly enhanced through the formation of doped $LaCrO_3$/YSZ composites.

4. Conclusions

The electrical conductivities of $LaCrO_3$, $(La_{1-x}M_x)CrO_3$ (M = Mg, Ca, Ba for $x = 0.3$ and M = Sr for $x = 0.25$), and $(La_{0.75}Sr_{0.25})(Cr_{0.5}Mn_{0.5})O_3$ perovskites are measured from 500 to 800 °C in both oxidizing and reducing atmospheres. A-site doping is found to be effective in improving the electrical conduction of $LaCrO_3$ in both environments, particularly if properly doped. With a decrease in pO_2, the electrical conductivity of undoped and doped $LaCrO_3$ perovskites decreases while the activation energy increases, probably due to the formation of oxygen vacancies under a reducing environment. The high-electrical conductivity of Sr- and Ca-doped $LaCrO_3$, particularly in air, and their preliminary electrochemical performance demonstrates their potential as cathode materials for solid oxide fuel cells.

Acknowledgements

This project was sponsored by the Agency for Science, Technology and Research of Singapore (A Star) under SERC Grant No. 0421010081 and the National Science Foundation (NSF) of China under the project contract 50571038, the "863" high-tech project under contract 2006AA05Z148.

References

[1] S.C. Singhal, K. Kendall, High-Temperature Solid Oxide Fuel Cells: Fundamentals, Design and Applications, Elsevier, Oxford, 2004.
[2] S.P. Jiang, S.H. Chan, J. Mater. Sci. 30 (2004) 4405.
[3] S.W. Tao, J.T.S. Irvine, Nat. Mater. 2 (2003) 320.
[4] Y.H. Huang, R.I. Dass, Z.L. Xing, J.B. Goodenough, Science 312 (2006) 254.
[5] J.C. Ruiz-Morales, J. Canales-Vázquez, C. Savanie, et al., Nature 439 (2006) 568.
[6] S.P. Jiang, X.J. Chen, S.H. Chan, J.T. Kwok, K.A. Khor, Solid State Ionics 177 (2006) 149.
[7] S.P. Jiang, X.J. Chen, S.H. Chan, J.T. Kwok, J. Electrochem. Soc. 153 (2006) A850.
[8] P. Vernoux, E. Djurado, M. Guillodo, J. Am. Ceram. Soc. 84 (2001) 2289.
[9] J.C. Ruiz-Morales, J. Canales-Vázquez, J. Pena-Martínez, D.M. López, P. Núnez, Electrochim. Acta 52 (2006) 278.
[10] R.D. Shannon, Acta Crystallogr. A 32 (1976) 751.
[11] S. Srilomsak, D.P. Schilling, H.U. Anderson, in: S.C. Singhal (Ed.), Proceedings of the First International Symposium on Solid Oxide Fuel Cells, The Electrochemical Society, Pennington, NJ, 1989, p. 129.
[12] M. Mori, T. Yamamoto, H. Itoh, T. Watanabe, J. Mater. Sci. 32 (1997) 2423.
[13] V.M. Goldschmidt, Geochemische Verteilungsgesetze der Elemente VII–VIII, Norske Videnskaps Akademi, Oslo, Skrifter, 1926.
[14] H. Moriwake, I. Tanaka, K. Tatsumi, et al., Mater. Trans. 43 (2002) 1456.
[15] P. Duran, J. Tartaj, F. Capel, et al., J. Eur. Ceram. Soc. 24 (2004) 2619.
[16] M. Mori, T. Yamamoto, T. Ichikawa, Y. Takedo, Solid State Ionics 148 (2002) 93.
[17] T. Ishihara, H. Matsuda, Y. Takita, J. Am. Chem. Soc. 116 (1994) 3801.
[18] M. Mori, T. Yamamoto, H. Itoh, T. Abe, et al., in: U. Bossel (Ed.), Proceedings of the First International Symposium on Solid Oxide Fuel Cell Forum, Lucerne, 1994, p. 465.
[19] J. Sfeir, P.A. Buffat, P. Möckli, N. Xanthopoulos, R. Vasquez, H.J. Mathieu, J.V. Herle, K.R. Thampi, J. Catal. 202 (2001) 229.
[20] J.H. Ouyang, S. Sasaki, T. Murakami, et al., Ceram. Int. 31 (2005) 543.
[21] R. Koc, H.U. Anderson, J. Mater. Sci. 27 (1992) 5477.
[22] J. Yoo, A. Verma, A.J. Jacobson, in: T.A. Ramanarayanan (Ed.), Ionic and Mixed Conducting Ceramics IV, The Electrochemical Society Inc., 2001, p. 27.
[23] I. Yasuda, T. Hikita, in: S.C. Singhal, H. Iwahara (Eds.), Proceedings of the Third International Symposium on Solid Oxide Fuel Cells, The Electrochemical Society, Hawaii, 1993, p. 354.
[24] C.N.R. Rao, B. Raveau, Transition Metal Oxides: Structure, Properties, and Synthesis of Ceramic Oxides, 2nd ed., Wiley–VCH, New York, 1998.
[25] D.B. Meadowcroft, in: T. Gray (Ed.), Proceedings of the International Conference on Strontium Containing Compounds, Atlantic Research Institute, Halifax, Canada, June, 1973, pp. 119–136.
[26] G.V.S. Rao, B.M. Wanklyn, C.N.R. Rao, J. Phys. Chem. Solids 32 (1971) 345.
[27] I. Yasuda, T. Hikita, in: F. Grosz, P. Zegers, S.C. Singhal, O. Yamamoto (Eds.), Proceedings of the Second International Symposium on Solid Oxide Fuel Cells, Commission of the European Communities, Athen, 1991, p. 645.
[28] K.P. Ong, P. Wu, L. Liu, S.P. Jiang, Appl. Phys. Lett. 90 (2007), Article no. 044109.
[29] Y. Kunifusa, M. Yoshinaka, K. Hirota, O. Yamaguchi, Solid State Ionics 149 (2002) 107.
[30] J. Zaannen, G.A. Sawatzky, J.W. Allen, Phys. Rev. Lett. 55 (1985) 418.
[31] G.A. Sawatzky, J.A. Allen, Phys. Rev. Lett. 53 (1984) 2339.
[32] J. Zaanen, G.A. Sawatzky, J. Solid State Chem. 88 (1990) 8.

[33] J.B. Torrance, P. Lacorre, C. Asavaroengchai, R.M. Metzger, Physica C 182 (1991) 351.
[34] G. Pari, S. Mathi Jaya, G. Subramoniam, R. Asokamani, Phys. Rev. B 51 (1995) 16575.
[35] P. Mahadevan, N. Shanthi, D.D. Sarma, J. Phys. Condens. Matter 9 (1997) 3129.
[36] P. Ravindran, A. Kjekshus, H. Fjellvåg, A. Delin, O. Eriksson, Phys. Rev. B 65 (2002) 64445.
[37] D. Muñoz, N.M. Harrison, F. Illas, Phys. Rev. B 69 (2004) 85115.
[38] H. Tagawa, J. Mizusaki, Y. Arai, Y. Kuwayama, S. Tsutiya, T. Takeda, S. Sesido, Denki Kagaku Oyobi Kogyo Butsuri Kagaku 58 (1990) 512.